Computational Time Reversal Ultrasonic Array Imaging of Multipoint Targets

Peter Simko
Dept. of Electrical and Computer Engineering
Illinois Institute of Technology
Chicago, Illinois 60616–3793
Email: psimko@ece.iit.edu

Jafar Saniie
Dept. of Electrical and Computer Engineering
Illinois Institute of Technology
Chicago, Illinois 60616–3793
Email: sansonic@ece.iit.edu

***Abstract*—In computational time reversal (CTR) ultrasonic imaging of point scatterers, the singular value decomposition of the response matrix is of critical importance. Determination of response matrix rank using singular value decomposition (SVD) is the first step in obtaining the null subspace projection operator which is used to quantify the contribution of a test illumination vector to the measured response matrix. The null subspace projection operator is formed from the summed outer products of the singular vectors associated with singular values of zero magnitude. For imaging in noisy environments or inhomogeneous media, singular values do not generally attain zero magnitude and we face the problem of correctly determining the identities of the singular vectors that span the signal subspace. Failure to correctly determine response matrix rank will result in a projection operator that either incompletely spans the actual noise subspace, or erroneously spans part of the signal subspace. This paper will provide physical justification for the observed loss of rank in the response matrix at low frequencies and develop a robust, efficient algorithm to determine the correct subspace dimensionality for generation of the null subspace projection operator in DORT-based CTR imaging algorithms. However, while successive singular values of the decomposition are guaranteed to be monotonically non-increasing, numerical simulations typically show that singular values do not correlate well to the actual scatterer reflectivities. The computed singular values may decrease in value very rapidly, so that even for a system with M equally reflective targets the Mth singular value may take on small values near zero. In general, the rank of the response matrix at a given frequency is only maximally given by the number of point targets being probed, and a robust and computationally efficient thresholding method is required to maximize imaging efficiency of CTR algorithms. We demonstrate using numerical simulations the efficiency of the thresholding algorithm. Imaging error introduced by suboptimal rank determination of the response matrix is quantified. We also quantify the effect of signal noise on image quality through its effect on rank determination accuracy.**

I. Introduction

Computational time reversal (CTR) imaging methods provide a potential means of obtaining true volumetric ultrasonic images from a relatively simple experimental system [1]. Possible applications for methods under consideration in this article include location of very small, approximately spherical targets in homogeneous or weakly inhomogeneous media. These criteria are met by targets such as small calcifications within human breast tissue, submerged sea mines in deep water and flaws in metal or ceramic materials. One of the most beneficial aspects of CTR is its ability to take advantage of the self-averaging property of weakly inhomogeneous media in order to improve cross-range resolution [2]. However, CTR imaging methods still present considerable challenges to be overcome, such as poor range resolution, difficulty imaging extended targets using finite-extent transducer arrays, and very high computational cost. This article will focus on one particular CTR imaging method: the DORT (*Décomposition de l'op 'erateur de retournement temporel*) [3] method, which is critically reliant on determination of the dimensionality of the null subspace obtained through eigenvalue decomposition of the multistatic response (MSR) matrix. Determination of null subspace rank is essentially related to but not identical with the problem of determining the number of point scatterers embedded within a surrounding medium. This paper considers the problem of targets embedded in homogeneous media in the presence of moderate additive white noise, but the results can be extended to weakly inhomogeneous media such as biological tissue.

The DORT method relies on the singular value decomposition (SVD) of the MSR matrix to differentiate between the signal and noise subspaces $\mathcal{S}$ and $\mathcal{N}$, the union of which is spanned by the component vectors of the MSR matrix. Conservation of energy dictates that the sum of the squares of the measured singular values must be equal to the total power scattered by the illuminated targets, plus noise terms. The key to DORT is the formulation of a null subspace projection operator which determines the proportionality between signal and null subspace components of an arbitrary, artificially generated illumination vector corresponding to a single hypothesized scatterer at an arbitrary test location. This operator is the outer product of those singular values likely to represent noise terms in the SVD (i.e. those singular vectors associated with relatively small singular values). Image quality is then influenced by the accuracy with which we assign the singular vectors to the null or signal subspaces of the MSR matrix: if we associate too many singular vectors with the null subspace then the rank of projection operator will be too high, causing the method to overestimate the noise contribution of the test vectors. It is therefore important to examine the properties of the decomposed MSR matrix and determine a reliable noise-based thresholding method yielding

1051-0117/07/$25.00 ©2007 IEEE

accurate null subspace rank. This paper examines the impact of suboptimal subspace rank estimation (over or under estimation of subspace dimensionality) on image quality.

II. Background

Essentially, the DORT method is an extension of the MUSIC algorithm to broadband imaging systems [4]. For simplicity we will consider a two dimensional system consisting of a collection of distinct point scatterers embedded in a homogeneous medium. Transducers are assumed to be ideal and point-like. Targets are illuminated by a series of pulses emitted by a set of N equally spaced transducers with pitch δ arranged in a static, one dimensional array with locations denoted by $\boldsymbol{x}_p$, $p = 1, \ldots, N$. Propagation of an impulse through the surrounding medium between points $\boldsymbol{r}, \boldsymbol{r}'$ is modeled using the frequency domain Green's function $G(\boldsymbol{r}, \boldsymbol{r}')$:

$$G(\boldsymbol{r}, \boldsymbol{r}') \equiv -\frac{e^{ik|\boldsymbol{r}-\boldsymbol{r}'|}}{4\pi|\boldsymbol{r}-\boldsymbol{r}'|}, \tag{1}$$

where k is the wavenumber. The total wave field ψ due to a pulse emitted by a single transducer at $\boldsymbol{x}_0$ scattered by M targets at locations $\boldsymbol{y}_m$, $m = 1, \ldots, M$ with real-valued reflectivities τ_m is expressed

$$\psi(\boldsymbol{r}) = \sum_{m=1}^{M} G(\boldsymbol{r}, \boldsymbol{y}_m)\tau_m G(\boldsymbol{y}_m, \boldsymbol{x}_0). \tag{2}$$

The region to be imaged is probed by performing N independent experiments, each consisting of emission of a pulse from the jth transducer and allowing sufficient time for all backscattered echoes to die out before emitting a pulse from the $(j+1)$th transducer. The illumination vector defined as

$$\boldsymbol{g}(\boldsymbol{r}) \equiv [G(\boldsymbol{x}_1, \boldsymbol{r}), G(\boldsymbol{x}_2, \boldsymbol{r}), \ldots, G(\boldsymbol{x}_N, \boldsymbol{r})]^T, \tag{3}$$

expresses the response at each array element $\boldsymbol{x}_i$ due to a single pulse emitted from $\boldsymbol{r}$. Representing the MSR matrix as $\boldsymbol{K}$, the vector in the jth column $\boldsymbol{K}_j$ represents the signals received at each transducer due a pulse emitted by the nth transducer and reflected by each of the embedded targets:

$$\boldsymbol{K}_j = \sum_{m=1}^{M} \tau_m G(\boldsymbol{x}_j, \boldsymbol{y}_m)\boldsymbol{g}(\boldsymbol{y}_m). \tag{4}$$

Using the Green's function definition of Eq. (1) we can make simple observations regarding the qualitative properties of the complex-valued illumination vectors. Expressing the illumination vector associated with a target at $\boldsymbol{y}$ in the form

$$\boldsymbol{g}(\boldsymbol{y}) = \frac{1}{4\pi}\begin{pmatrix} |\boldsymbol{x}_1 - \boldsymbol{y}|^{-1} \cdot e^{ik|\boldsymbol{x}_1-\boldsymbol{y}|} \\ \vdots \\ |\boldsymbol{x}_N - \boldsymbol{y}|^{-1} \cdot e^{ik|\boldsymbol{x}_N-\boldsymbol{y}|} \end{pmatrix}, \tag{5}$$

we see that the component magnitudes are frequency independent and vary smoothly as $\boldsymbol{x}_j$ takes on all values across subscript j. Furthermore, for the imaging arrangement under consideration there are only three general interrelationships:

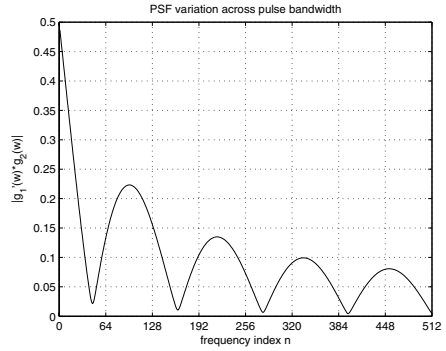

Fig. 1. PSF magnitudes vs. frequency

i. & ii. The magnitudes $|\boldsymbol{x}_j - \boldsymbol{y}|^{-1}$ may be monotonically increasing (resp. decreasing) with increasing transducer index j for a target positioned in the upper (resp. lower) half-plane with respect to the array axis.

iii. For a target positioned sufficiently close to the array axis the magnitudes will show an approximately parabolic curve (opening downward).

Since a large proportion of the information differentiating the illumination vectors of a pair of scatterers $\boldsymbol{y}$ and $\boldsymbol{y}'$ located within the same half-plane is contained within the component phase terms, we expect the inner product of the illumination vectors to show distinct features at low frequencies. The inner product is called the point spread function (PSF) and is defined as

$$\Gamma(\boldsymbol{y}, \boldsymbol{y}') = \boldsymbol{g}^H(\boldsymbol{y})\boldsymbol{g}(\boldsymbol{y}'). \tag{6}$$

This expression describes the field at $\boldsymbol{y}'$ due to an impulse emitted from $\boldsymbol{y}$ and backpropagated into the medium by the transducer array. As an example, Figure 1 shows the plot of the of the magnitude the PSF for $\boldsymbol{y} = (30, 3)\lambda_c$, $\boldsymbol{y}' = (30, 13)\lambda_c$, where λ_c is the central pulse wavelength. The array consists of 17 transducers with pitch $\delta = 0.5\lambda_c$. Note here that the lowest discrete frequency in the pulse bandwidth is not equal to zero (details to be given in section IV). In the figure, the magnitudes of the inner products vary in a largely periodic manner, often taking on values considerably larger than 0.

Computational imaging methods rely on the mathematical backpropagation of a test illumination vector to form the coherent image of the total wave field ψ. For a simplified problem consisting of a single target ($M = 1$) at $\boldsymbol{y}$ probed by N transducers, the backpropagated field H at $\boldsymbol{r}$ due to a target illuminated by a single transducer $\boldsymbol{x}_k$ is directly related to the PSF via

$$\begin{aligned} H(\boldsymbol{r}, \boldsymbol{y}) &= \sum_{j=1}^{N} \overline{G(\boldsymbol{r}, \boldsymbol{x}_j)}\, G(\boldsymbol{x}_k, \boldsymbol{y})\, G(\boldsymbol{y}, \boldsymbol{x}_j) \\ &= G(\boldsymbol{y}, \boldsymbol{x}_k)\, \Gamma(\boldsymbol{r}, \boldsymbol{y}). \end{aligned} \tag{7}$$

By assuming targets located in the far-field and approximately equidistant from the array at a distance h, we can approximate the PSF in the manner of Devaney [5], beginning with an

asymptotic model of the Green's function for a target at $\boldsymbol{y} = (x, y)$ a distance $y = h$ from an array with inter-element pitch δ:

$$G(\boldsymbol{y}, \boldsymbol{x}_n) \approx -\frac{1}{4\pi h} e^{ik(h+(x^2+(n\delta)^2)/2h)} e^{-ik(\frac{xn\delta}{h})}. \quad (8)$$

which yields the PSF approximation

$$\Gamma(\boldsymbol{y}, \boldsymbol{y'}) = \frac{1}{(4\pi h)^2} e^{ik(\frac{x^2-x'^2}{2h})} \sum_{n=1}^{N} e^{ik(\frac{n\delta}{j})(x'-x)}. \quad (9)$$

Eq. (9) indicates that $\Gamma(\boldsymbol{y}, \boldsymbol{y'}) = 0$ only when the summation term is equal to zero (and $x \neq x'$). With these approximations, this equation also predicts the locations of minima apparent in Figure 1 to about 3%.

A direct consequence of the non-orthogonality of illumination vectors in the presence of noise is an apparent variability of the dimensionality of the noise subspace across the bandwidth of the pulse. The SVD algorithm ensures that singular values follow the relation $\sigma_1 \geq \sigma_2 \geq \cdots \geq \sigma_n$. In noise-free environments, $\sigma_r(\omega) = 0$ for $r > M$, but in the presence of noise the higher indexed singular values take decreasing but uniformly non-zero values. The values of r at which $\sigma_r(\omega)$ become very near zero tend to vary across the pulse bandwidth.

Recall that the vectors of the MSR matrix span a total space $\mathcal{C}$ representable as

$$\mathcal{C} = \mathcal{S} \oplus \mathcal{N}, \quad (10)$$

with $\mathcal{S}$ and $\mathcal{N}$ the signal and noise subspaces respectively. A critical component of the DORT method is the null subspace projection operator $\mathscr{P}$, which determines the component of a generalized test illumination vector parallel to the noise subspace [2], [4]. The operator $\mathscr{P}$ is computed by summing the outer products of the singular vectors spanning the signal subspace and subtracting the result from the $N \times N$ identity matrix $\boldsymbol{I}$:

$$\mathscr{P}(\omega) = \boldsymbol{I} - \sum_{r=1}^{M} U_r(\omega) U_r^H(\omega), \quad (11)$$

where the subscript r takes the indices of those singular values sufficiently greater than zero. A more precise definition of "sufficiently greater than" will be provided in the next section. Due to symmetry of $\boldsymbol{K}$, the singular vectors U of $\boldsymbol{K}$ are parallel to the eigenvectors of $\boldsymbol{K}$. From symmetry and the conservation of power, it may be shown that in the absence of noise, the sum of the squares of the eigenvalues of $\boldsymbol{K}$ is equivalent to the sum the magnitudes of the component column vectors. The columns of $\boldsymbol{K}$ are in turn linear combinations of M illumination vectors, each of magnitude proportional to scatter reflectivity τ_m. However, while the singular vectors of $\boldsymbol{K}$ with non-zero associated singular values are guaranteed to be orthogonal and span the signal subspace (i.e., the complement of the null subspace), it is apparent from the non-orthogonality of the illumination vectors that the singular values will not generally correspond to the magnitudes of the component vectors of $\boldsymbol{K}$ (and by extension the reflectivities τ_m). For example, if we consider the simple case of two equally reflective targets in a noise-free environment with nearly parallel illumination vectors, the SVD of $\boldsymbol{K}$ will yield a pair of non-zero singular values where the difference $\sigma_1 - \sigma_2$ is potentially much larger than the difference in illumination vector magnitudes.

III. Null Subspace Rank

In noise-free environments, associated singular value/vector pairs are related in a one-to-one manner to discrete, well-separated targets [6]. In the presence of noise all singular values $\sigma_r(\omega)$ of $\boldsymbol{K}$ take on non-zero values, although for all $\sigma_r(\omega)$, $r > M$ we expect the values to be near zero. Due to non-orthogonality, we cannot assume that all $\sigma_r(\omega)$ will be above some noise-determined threshold for all $r \leq M$. Therefore, we introduce the *estimated rank* of $\boldsymbol{K}$ to be equivalent to the number of singular values above some run-time determined threshold that is generally dependent on the noise profile of the transducers. The estimated rank is frequency dependent and is generally less than or equal to M, rather than uniformly M across the entire pulse band. Two factors contribute to the apparent rank variability in noisy broadband applications. First, there is the non-orthogonality of illumination vectors discussed in the previous section. There is also the non-uniform distribution of signal power over the pulse band. Our simulations use a band-limited pulse with central frequency ν of the form

$$f(t) = -2\pi^2\nu^2(t-\nu^{-1})e^{-\pi^2\nu^2(t-\nu^{-1})^2}. \quad (12)$$

At frequencies far from the center of the pulse band, the SNR decreases substantially from the maximal value near the center of the band, resulting in a reduced dimensionality of the signal subspace.

This apparent reduction in null subspace dimensionality at certain frequencies should be considered in any DORT-based imaging algorithm. While DORT is generally a robust algorithm even in the presence of inhomogeneous scattering media, we cannot rely on *a priori* knowledge of M for general imaging problems and so must be able to reliably extract an estimate of the null subspace rank after performing the singular value decomposition of $\boldsymbol{K}$.

Our rank determination method begins with the observation that the measured power at any frequency is approximately the sum of the total reflected power and white noise power P_w. It can be shown that due to the complex symmetric nature of the MSR, the magnitudes of the column vectors K_n are related to the singular values through the relation

$$\sum_{n=1}^{N} \sigma_n^2 = \sum_{n=1}^{N} \|K_n\|^2. \quad (13)$$

We assume that for a given experimental apparatus the SNR will generally be known and noise power P_w is constant across the pulse bandwidth. Then, taking the total measured power

$P_m(\omega)$:

$$P_m(\omega) = \sum_{n=1}^{N} \sigma_n^2(\omega) = P_s(\omega) + P_w \tag{14}$$

so that $P_w = \text{SNR}^{-1} \cdot P_s(\omega)$. Solving for $P_s(\omega)$ gives us

$$P_s(\omega) = \frac{P_m(\omega)}{(1 + \text{SNR}^{-1})}. \tag{15}$$

Eq. 15 tells us how many singular vectors to include in the outer product summation of Eq. 11. At each discrete frequency in the plots of singular value vs. frequency, find the minimum value of T such that $\sum_{n=1}^{T} \sigma_n^2(\omega) \geq P_s(\omega)$, then replace the summation variable M in Eq. 11 with T. In the next section we present results demonstrating that the DORT method allows some variation in T from the expected value $T = M$ while still maintaining good image quality.

IV. Simulation Results

Figure 2 shows the first five singular value traces for four equally reflective targets probed with an array consisting of eight transducers with pitch δ equal to twice the central pulse wavelength λ_c. All targets are located approximately $30\lambda_c$ from the array, with cross range locations $16\lambda_c$, $10\lambda_c$, $4\lambda_c$ and $-4\lambda_c$ from the array's central axis. Central pulse frequency is 3 MHz with 3.75 MHz bandwidth at -6dB. A large amount of additive Gaussian noise at $\text{SNR}_{dB} = 8$ has been applied to the simulated signal in order to properly illustrate the characteristics of the singular value plot for the noise-associated singular value $\sigma_5(\omega)$. The general trend is for the integrated plots of singular value vs. frequency for the first four singular values to take values substantially larger than the integral of $\sigma_5(\omega)$. We note that integral of each trace is less than that of the trace preceding it, despite the fact that our simulation is based on equally reflective scatterers placed at approximately equal distances from the array. Also, the fourth trace shows a substantial dip in power in bands centered near the 140th and 190th discrete frequencies.

Even near the peak of the pulseband power curve, the singular values may sometimes decrease in value rapidly with increasing r and the apparent signal subspace rank may be less than M. Near the edges of the band we also note a more gentle decrease in singular values with increasing r due to the nature of the pulseband power spectrum. In view of Fig. 2 and Eq. (11) and its associated algorithm description, we expect that as we approach the extreme edges of the pulse bandwidth we require higher values of T in order to sum over enough singular values. An example image obtained from the array/target system described above is shown in Fig. 3. The array element on the left side are marked by '$+$' characters, and the true locations of the embedded targets are marked with '$\times$' characters.

We quantify imaging efficiency by integrating the power contained in the synthesized image along a series of uniformly distributed radial lines originating at the array center, sweeping

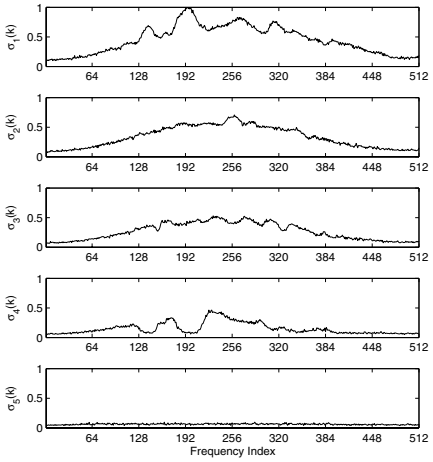

Fig. 2. Singular values vs. frequency, four targets illuminated by eight transducers (three highest index singular values omitted)

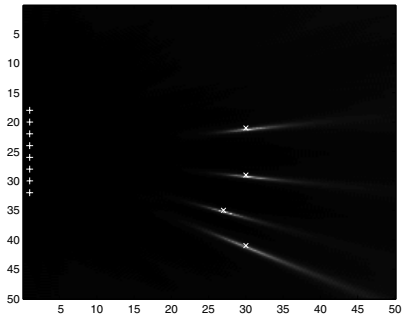

Fig. 3. Sample image obtained using DORT method

out a 180° arc. This method eliminates range information from consideration which is desirable since DORT is essentially a cross-range estimation method. Fig. 4 shows 4 power curves for the same target arrangement of Fig. 2 probed by a 15 element array (compared to 8 used to generate Fig. 2) of length $14\lambda_c$, pitch $\delta = \lambda_c$ with SNR=12dB. The dashed vertical lines show the actual angular positions of the simulated targets. In each subplot of Fig. 4 we have kept the null subspace rank constant across the pulse band: the uppermost plot uses a projection operator $\mathscr{P}$ obtained from Eq. (11) with $T = 2$ (overestimation of null subspace rank) replacing the summation limit M, and the middle and lower subplots use $T = 4$ and $T = 6$, respectively. This indicates that the penalty for underestimation of null subspace rank is small, at least for relatively small degrees of underestimation. Note that the power peak associated with the target near 97° is substantially lower than the other peaks due to non-orthogonality in each case. Fig. 4 suggests that we may be somewhat conservative with our rank estimation algorithm, reducing null subspace rank whenever we find ourselves in doubt as to whether a given set of singular vectors spans the signal subspace, without

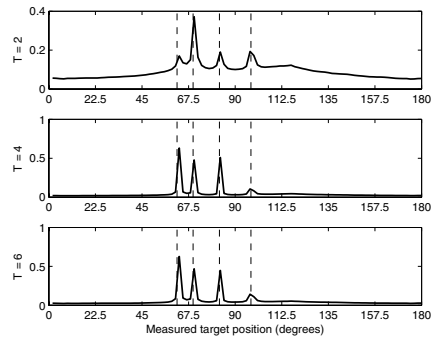

Fig. 4. Measured power distribution as a function of direction of arrival, four targets, simplified rank

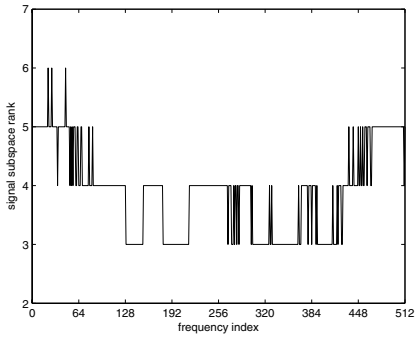

Fig. 6. Signal subspace rank vs. frequency

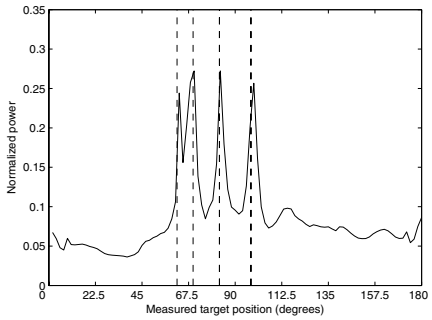

Fig. 5. Measured power distribution as a function of direction of arrival

sacrificing image quality. Finally, in Fig. 5 we see the power distribution for the same array and target arrangement, but with null subspace rank determined according to Eq. (15). Fig. 6 shows the frequency dependent values of T across the pulse band. The improvement in peak levels associated with the equally reflective targets may clearly be seen. The apparent trade-off is a higher noise level and poorer separation between peaks for scatterers at 64° and 69°.

V. Conclusion

We have shown how the DORT computational time reversal imaging method displays considerable robustness in the face of suboptimal null subspace rank determination. By taking into account the properties of the PSF across the frequency support of the broadband interrogation pulse, we have shown how this leads simply and directly to null subspace rank determination method that uses r singular vectors in constructing the projection operator, where r may generally be greater or less than M, the actual number of targets embedded in the medium. An improvement in imaging efficiency is observed over the more simplistic methods that assume constant null subspace rank across the pulse band. Future research efforts may include examination of the effect of inhomogeneities in the surrounding medium on rank determination and the effect of array geometry variation on image quality.

References

[1] C. Prada, E. Kerbrat, D. Cassereau, and M. Fink, "Time reversal techniques in ultrasonic nondestructive testing of scattering media," *Inverse Problems*, vol. 18, pp. 1761–1773, 2002.

[2] L. Borcea, G. Papanicolaou, C. Tsogka, and J. Berryman, "Imaging and time reversal in random media," *Inverse Problems*, vol. 18, pp. 1247–1279, 2002.

[3] C. Prada, S. Manneville, D. Spoliansky, and M. Fink, "Decomposition of the time reversal operator: Detection and selective focusing on two scatterers," *J. Accoust. Soc. Am.*, vol. 99, pp. 2067–2076, 1996.

[4] A. J. Devaney, "Super-resolution processing of multi-static data using time reversal and music," 2002, http://www.ece.neu.edu/faculty/devaney/.

[5] ——, "Time reversal imaging of obscured targets from multistatic data," *IEEE Trans. Antennas and Propag.*, vol. 53, no. 5, pp. 1600–1610, May 2005.

[6] C. Prada and M. Fink, "Eigenmodes of the time reversal operator: A solution to selective focusing in multiple-target media," *Wave Motion*, vol. 20, pp. 151–163, 1994.